

# Generative Pre-trained Autoregressive Diffusion Transformer

Yuan Zhang<sup>1\*</sup>, Jiacheng Jiang<sup>2\*</sup>, Guoqing Ma<sup>3\*†</sup>, Zhiying Lu<sup>4</sup>, Haoyang Huang<sup>3</sup>, Jianlong Yuan<sup>3</sup>,  
Nan Duan<sup>3‡</sup>, and Daxin Jiang<sup>3</sup>

<sup>1</sup>Peking University

<sup>2</sup>Tsinghua University

<sup>3</sup>StepFun, China

<sup>4</sup>University of Science and Technology of China

## Abstract

In this work, we present GPDiT, a Generative Pre-trained Autoregressive Diffusion Transformer that unifies the strengths of diffusion and autoregressive modeling for long-range video synthesis, within a continuous latent space. Instead of predicting discrete tokens, GPDiT autoregressively predicts future latent frames using a diffusion loss, enabling natural modeling of motion dynamics and semantic consistency across frames. This continuous autoregressive framework not only enhances generation quality but also endows the model with representation capabilities. Additionally, we introduce a lightweight causal attention variant and a parameter-free rotation-based time-conditioning mechanism, improving both the training and inference efficiency. Extensive experiments demonstrate that GPDiT achieves strong performance in video generation quality, video representation ability, and few-shot learning tasks, highlighting its potential as an effective framework for video modeling in continuous space.

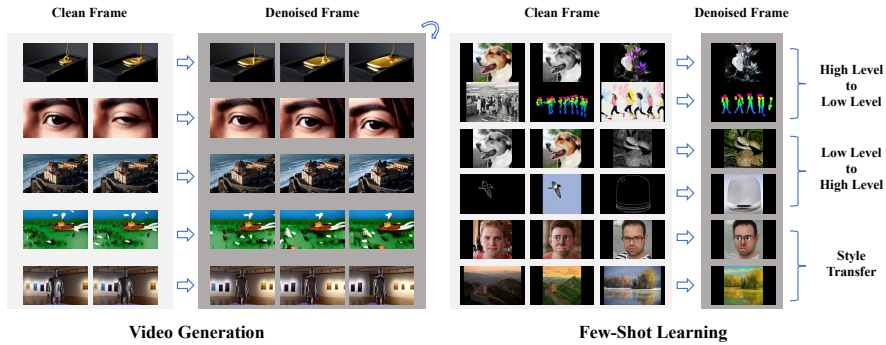


Figure 1: Video Generation and Few-Shot Multitask Learning. The left side of the figure illustrates the model’s video generation capability: given a set of initial frames, the model can continue the sequence by generating denoised frames. The right side showcases the model’s multitask learning ability, similar to the approach presented in [35]. After few-shot fine-tuning, the model is capable of performing a variety of tasks, such as translating high-level features to low-level features, converting low-level features to high-level features, and executing style transfer across video sequences.

\*Equal contribution.

†Technical leader.

‡Corresponding author.

# 1 Introduction

Diffusion models have achieved notable success in video generation [1, 2, 11, 14]. Despite recent advancements, existing diffusion-based approaches exhibit limitations in temporal consistency and motion coherence, particularly in long-range generation. A key contributing factor is the use of bidirectional attention. This allows future context to influence current predictions, thereby violating the causal structure required for autoregressive generation.

In contrast, autoregressive (AR) modeling has become the de facto paradigm in natural language processing [3, 34, 35]. This method inherently captures the causality in sequences by predicting the next token based on previously generated outputs, thereby facilitating both sequence modeling and structural understanding. Inspired by this, recent efforts [7, 9, 51] have focused on integrating AR modeling with diffusion processes to leverage their complementary strengths. This integration aims to improve temporal coherence and enhance motion continuity in extended video synthesis. Notably, compared to traditional cross-entropy objectives that explicitly train for next-token prediction, the combination of diffusion-based loss and AR modeling offers an implicit path to temporal understanding, serving as a natural byproduct rather than a specially designed objective.

One line of research investigates the replacement of bidirectional attention with causal attention [4, 8, 10, 16, 60] for improved modeling of temporal dependencies. Specifically, the attention computation restricts each noisy token to attend only to preceding clean tokens and itself. This architectural design enables more robust generalization to video lengths beyond those seen during training, whereas bidirectional attention often leads to severe quality degradation when extrapolating to longer sequences. Moreover, causal attention is naturally compatible with KV cache, significantly accelerating the generation of long sequences. These advantages are unattainable with traditional bidirectional attention mechanisms.

Another increasingly studied approach is diffusion forcing [5, 20, 39, 42], characterized by the asynchronous injection of token-specific noise levels during training to facilitate long-range dependency modeling. During inference, this method operates in a coarse-to-fine manner: it first generates early frames and then progressively refines later ones through iterative denoising. While promising, this paradigm still struggles with training instability, with independent frame-level noise schedules often impairing performance compared to synchronized alternatives.

To address the aforementioned challenges in long-sequence video modeling, we introduce Generative Pre-trained Autoregressive Diffusion Transformer (GPDiT), a frame-wise autoregressive diffusion framework. In contrast to discrete token-level autoregressive modeling, GPDiT captures causal dependencies across frames while preserving full attention within each frame, enabling both sequential coherence and intra-frame expressivity. Moreover, GPDiT improves training and inference efficiency through two practical architectural modifications. The first component introduces an attention mechanism that leverages the temporal redundancy of video sequences by eliminating attention computation between clean frames during training, thereby reducing computational cost without compromising generation performance. The second is a parameter-free time-conditioning strategy that reinterprets the noise injection process as a rotation in the complex plane defined by data and noise components. This design removes the need for adaLN-Zero [31] and its associated parameters, yet still effectively encodes time information. As shown in Figure 1, GPDiT performs well in both video generation and few-shot learning tasks.

Our main contributions can be summarized as follows:

- We introduce GPDiT, a strong autoregressive video generation framework that leverages framewise causal attention to improve temporal consistency over long durations. To further enhance efficiency, we propose a lightweight variant of causal attention that significantly reduces computational costs during both training and inference.
- By reinterpreting the forward process of diffusion models, we introduce a rotation-based conditioning strategy, offering a parameter-free approach to inject time information. This lightweight design eliminates the parameters associated with adaLN-Zero while achieving model performance on par with state-of-the-art DiT-based methods.
- Extensive experiments demonstrate that GPDiT achieves competitive performance on video generation benchmarks. Furthermore, evaluations on video representation tasks and few-shot learning tasks show its potential of video understanding capabilities.

## 2 Related works

**Video Diffusion models.** Diffusion and flow-based generative models [13, 23, 24, 40, 45, 53] have demonstrated unprecedented ability to capture visual concepts and produce high-quality images. Video Diffusion Models [14] is the first work to introduce diffusion models for video generation. However, the expense associated with pixel space diffusion and denoising is nontrivial, requiring substantial computational resources. Models such as Magicvideo [59] and LVDM [11] speed up training and sampling efficiency by compressing high-dimensional video data into a latent space. Recent efforts have scaled diffusion transformers to substantially larger capacities, demonstrating significantly enhanced generation capabilities and further revolutionizing the field of text-to-video (T2V) synthesis, driving rapid progress across a broad range of applications [15, 18, 22, 26, 27, 29, 30, 38, 43, 46, 47, 50, 57].

**Autoregressive Modeling.** An emerging trend is the integration of autoregressive modeling and diffusion models. A key characteristic of this approach is that the model predicts future videos based on previously generated content. Representative works, such as [21, 49, 48, 55, 58], leverage an additional visual tokenizer that maps pixel-space inputs into discrete tokens, which are then fed into a language model to generate videos. However, this mapping is inherently lossy, leading to inferior performance compared to video diffusion models. Recent works [10, 25, 42, 60], inspired by Diffusion Forcing [5], allow each video frame to be processed with distinct noise levels, enabling the generation of videos with variable lengths. However, adding noise to antecedent sequences complicates future predictions and degrades performance on discriminative tasks. Recent work [17] addresses this prediction ambiguity by preserving the clarity of antecedent representations, keeping them noise-free.

## 3 Preliminary

### 3.1 Denoising Diffusion

Diffusion models generate data by progressively corrupting samples from the data distribution with Gaussian noise, eventually transforming them into pure noise, and then learning to invert this process through a sequence of denoising steps. Formally, given a data distribution  $p_{\text{data}}(x)$ , diffusion models apply a stochastic differential equation (SDE) to gradually perturb the data:

$$dx_t = \mu(x_t, t) dt + \sigma(t) dw_t, \quad (1)$$

where  $t \in [0, T]$  for some fixed terminal time  $T > 0$ ,  $\mu(\cdot, \cdot)$  denotes the drift coefficient,  $\sigma(\cdot)$  is the diffusion coefficient, and  $\{w_t\}_{t \in [0, T]}$  represents a standard Brownian motion. Let  $p_t(x)$  denote the marginal distribution of  $x_t$ ; by construction, the initial distribution satisfies  $p_0(x) = p_{\text{data}}(x)$ . A notable property of this SDE is the existence of a corresponding ordinary differential equation (ODE), referred to as the Probability Flow ODE [40], whose solution trajectories are guaranteed to match the time-evolving marginals  $p_t(x)$ :

$$dx_t = \left[ \mu(x_t, t) - \frac{1}{2} \sigma(t)^2 \nabla \log p_t(x_t) \right] dt. \quad (2)$$

## 4 Generative Pre-trained Autoregressive Diffusion Transformer (GPDiT)

In this section, we present an effective framework that combines autoregressive and diffusion models for video modeling. First, we introduce two variants of the attention mechanism tailored for frame-aware autoregressive diffusion in Section 4.1. Then, we discuss a flexible conditioning strategy designed to handle both clean and noisy frames in Section 4.2. Figure 2 provides an overview of the GPDiT framework, illustrating the inference pipeline, the internal architecture of a GPDiT block, and the rotation-based interpretation of the diffusion process.

### 4.1 Attention mechanism

#### 4.1.1 Vanilla Causal Attention

The traditional bidirectional attention mechanism has been criticized for disrupting temporal coherence and failing to maintain consistency in long video modeling. Meanwhile, most existing models

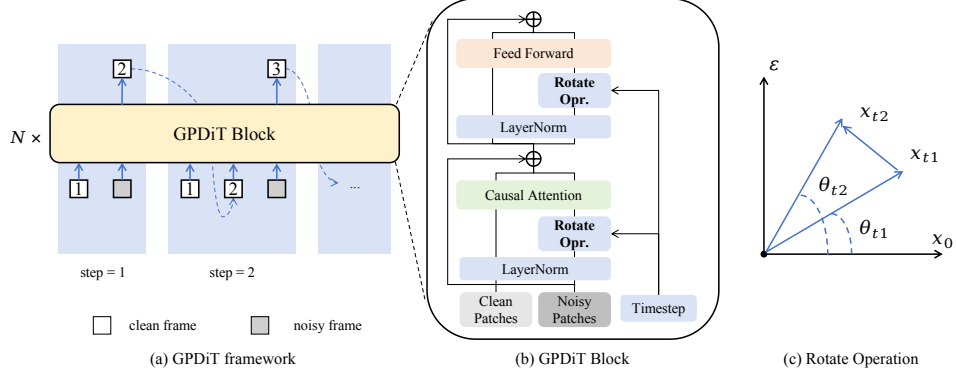


Figure 2: *Left plane*: An overview of GPDiT inference. *Middle plane*: The architecture of a typical GPDiT block, where adaLN-Zero is replaced with our rotation-based time conditioning, and causal attention is adopted instead of conventional bidirectional attention. *Right plane*: An illustration of the rotation-based view of the diffusion forward process, where the data and noise components evolve through a parameter-free rotation in the complex plane.

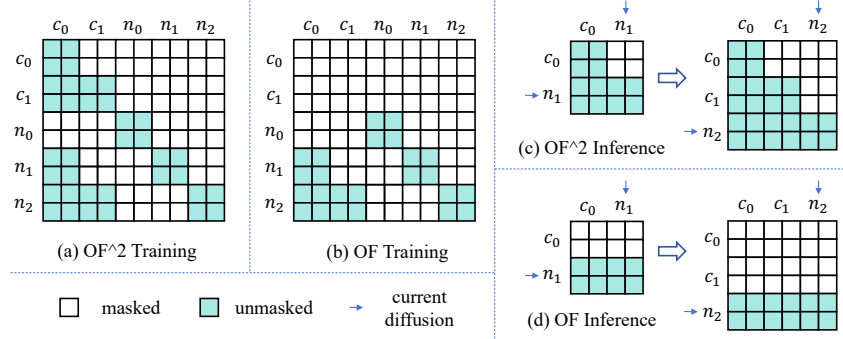


Figure 3: Illustration of two causal attention variants. Both apply intra-frame full attention and inter-frame causal attention, but differ in cross-frame attention handling between clean frames.  $c_i$  and  $n_i$  denote clean and noisy frames, respectively.

struggle to produce high-quality videos that exceed the frame length they were trained on since the models can only learn the joint distribution of fixed-length frames. To alleviate the issues, we employ the standard causal attention shown in Figure 3 (a) and (c), where each noisy frame  $n_i$  can only attends to previous clean frames  $c_{<i}$  and itself, while  $c_{<i}$  also attend to each other. The training objective is:

$$\mathcal{L}(\theta) = \mathbb{E}_{t \sim U[0,1], \epsilon \sim \mathcal{N}(0,I), x \sim p_{data}} \|\epsilon(n_i, t | c_{<i}) - \epsilon^t\|^2. \quad (3)$$

A notable advantage of standard causal attention is its compatibility with key-value (KV) caching [33] during inference, significantly accelerating generation and shortening the time needed for long video production.

#### 4.1.2 Lightweight Causal Attention

Although the advantages of vanilla causal attention are notable, it presents two major challenges. First, during training, maintaining a clean copy of the noised sequence for attention map computation doubles the memory and computational costs. Second, during inference, the inevitable expansion of the KV cache due to token accumulation in long-sequence prediction imposes a prohibitive memory burden.

To address these issues, we propose a lightweight causal attention mechanism that exploits the spatial redundancy in video data. As illustrated in Figures 3 (b) and (d), we eliminate attention score computation between clean frames, thus reducing additional operations without compromising model performance. To quantify computational savings, we analyze the attention complexity in the vanilla design. The computational overhead can be decomposed into three components: attention

between clean contexts, attention between noisy frames and clean contexts, and self-attention among noisy frames, with computational complexities of  $\mathcal{O}(\frac{1}{2}F^2)$ ,  $\mathcal{O}(\frac{1}{2}F^2)$ , and  $\mathcal{O}(F)$ , respectively, where  $F$  denotes the number of frames. Since attention between clean frames accounts for nearly half of the total computation, its removal leads to a substantial reduction in training cost. Moreover, during inference, achieving  $\mathcal{O}(F)$  complexity with standard causal attention requires maintaining a key-value (KV) cache, resulting in an additional  $\mathcal{O}(2F)$  memory overhead. In contrast, our method attains  $\mathcal{O}(F)$  inference complexity without incurring extra memory costs, substantially reducing the memory footprint.

## 4.2 Re-Thinking Timestep Conditioning Injection

The Adaptive Normalization Layer Zero (adaLN-Zero) has been widely utilized to incorporate timestep and class-label embeddings into diffusion model backbones, as introduced in DiT [31]. adaLN-Zero is typically designed as an MLP block to extract class-label embeddings for each transformer block. However, modern tasks in text-to-image, text-to-video, and image-to-video generation involve more complex semantic embeddings. These embeddings are often injected into the model through techniques such as token concatenation along the sequence dimension or cross-attention, leaving the MLP block to primarily handle timestep embeddings. The authors of [6] argue that the adaLN-Zero submodule contributes significantly to the model’s parameter count, accounting for an increase of approximately 28%. This considerable overhead has motivated research into more efficient methods for incorporating time conditioning in these models, aiming to reduce the computational cost while maintaining or enhancing performance.

We begin by considering the forward (variance-preserving) diffusion process, given by:

$$x_t = \sqrt{\alpha_t}x_0 + \sqrt{1 - \alpha_t}\epsilon,$$

where  $x_0 \in \mathbb{R}^D$  is a clean sample drawn from the data distribution,  $\epsilon \sim \mathcal{N}(0, I)$  represents standard Gaussian noise, and  $\alpha_t \in [0, 1]$ . To facilitate our analysis, we reduce the problem to one dimension ( $D = 1$ ) and reinterpret the forward process as a rotation in a 2D space. Specifically, we define the rotation angle  $\theta_t$  as:

$$\cos \theta_t = \sqrt{\alpha_t}, \quad \sin \theta_t = \sqrt{1 - \alpha_t},$$

such that the forward process becomes:

$$x_t = \cos \theta_t x_0 + \sin \theta_t \epsilon.$$

To represent this process geometrically, we stack the clean sample  $x_0$  and the noise  $\epsilon$  into a 2-vector  $\begin{pmatrix} x_0 \\ \epsilon \end{pmatrix} \in \mathbb{R}^2$ . The forward diffusion step is then represented as an orthogonal rotation in this 2D space:

$$\begin{pmatrix} x_t^{(0)} \\ x_t^{(1)} \end{pmatrix} = \underbrace{\begin{pmatrix} \cos \theta_t & \sin \theta_t \\ -\sin \theta_t & \cos \theta_t \end{pmatrix}}_{R(\theta_t)} \begin{pmatrix} x_0 \\ \epsilon \end{pmatrix},$$

In this formulation,  $x_t^{(0)}$  represents the usual diffused sample, while  $x_t^{(1)}$  is its orthogonal complex companion. The clean sample  $x_0$  and the noise  $\epsilon$  can be recovered by applying the inverse rotation:

$$\begin{pmatrix} x_0 \\ \epsilon \end{pmatrix} = R(\theta_t)^{-1} \begin{pmatrix} x_t^{(0)} \\ x_t^{(1)} \end{pmatrix}.$$

The model is trained to predict the complex companion  $x_t^{(1)}$  from the input  $x_t^{(0)}$  using a predefined loss function, which is assumed to be unknown for the current analysis.

The proposed approach follows the principle of parsimony, applying a reverse rotation with the angle  $\theta_t$  on  $x_t^{(0)}$  for each block to efficiently inject the timestep embedding while incurring no additional computational overhead. Other forms of conditioning, such as text or image conditioning, can be incorporated in the standard manner.

## 5 Experiments

### 5.1 Experimental Setups

We conduct experiments in three scenarios: video generation, video representation, and few-shot learning. The results demonstrate that GPDiT exhibits excellent generative and representational capabilities, which are crucial for building a unified model for visual understanding and generation, as well as the ability to transfer to downstream tasks with minimal cost and no need for additional modules.

**Datasets.** For video generation task, UCF-101 [41] dataset consists of 13,320 videos across 101 action categories and is widely used for human action recognition, MSR-VTT [52] is a large-scale dataset designed for open-domain video captioning, containing 10,000 video clips from 20 categories, with each clip annotated with 20 English sentences by Amazon Mechanical Turk workers. We assess the capability of GPDiT in video representation on the UCF-101 dataset. For the few-shot learning tasks, we construct multiple supervised fine-tuning (SFT) datasets. For each task, we create a SFT dataset with 20 video sequences, each generated by sampling three pairs from a set of 40 task-specific image pairs. These tasks include human detection, image colorization, Canny edge-to-image reconstruction, and two style transfer applications.

**Evaluations.** For video generation, we randomly sample 10,000 videos from UCF-101 and 7,000 videos from MSR-VTT. The Fréchet Video Distance (FVD) [44] is computed for entire videos, while the average Fréchet Inception Distance (FID) [12] and Inception Score (IS) [36] are calculated over individual frames. For the video representation task, top-1 accuracy is reported using a linear probing protocol. In the few-shot learning setting, we provide per-task video results along with qualitative analyses.

**Implementation details.** To ensure fair comparison, we design a benchmark model with 80 million parameters based on the architecture in Table 1. Trained on UCF-101, each video is center-cropped and resized to  $256 \times 256$ . The Adam optimizer with a learning rate of  $1e-4$  and a total batch size of 96 across 32 H100 GPUs is used. Training lasts for 400k iterations.

Table 1: Model variants of GPDiT. We follow the model size configurations of DiT [31] and SiT [28], replacing adaLN-Zero with a parameter-free rotation-based time conditioning.

Models	#Layers	Hidden Size	MLP	#Heads	#Params
GPDiT-B	12	768	3072	12	85M
GPDiT-H	24	2816	11264	22	2B

We further scale the model to a two-billion-parameter variant, GPDiT-H (see Table 1). First, we perform a 200k-iteration warm-up using an unconditioned image dataset from LAION-Aesthetic [37] with a learning rate of  $1e-4$  and batch size of 960. Training continues for another 200k iterations on a mixed image-video dataset, with equal sampling of images and videos, and batch sizes of 256 and 64, respectively. Video frames are sampled every three frames and clipped into 17-frame segments. Each image is center-cropped to the resolution closest to the original, with target sizes of  $256 \times 256$ ,  $192 \times 320$ , or  $320 \times 192$ , and video to  $192 \times 320$ . Finally, we continue training the GPDiT-H model on a pure video dataset featuring variable video lengths ranging from 17 to 45 frames. This stage lasts for an additional 150k iterations, using a reduced learning rate of  $2e-5$ . The resulting model is denoted as GPDiT-H-LONG. To compress video latents, we employ WanVAE [45], which reduces four frames into a single latent representation.

### 5.2 Video Generation

To evaluate the generalization ability of the GPDiT framework, we conduct experiments on two zero-shot video generation tasks: MSR-VTT and UCF-101 using GPDiT-H. The training data does not overlap with the test datasets, allowing us to assess the model’s ability to generalize to unseen data. At the same time, to assess its fitting capability, we trained the GPDiT-B model on UCF-101 and measured its generation performance. For both models, 12-frame video sequences are generated, conditioned on 5 input frames. The generated results are evaluated using FID, FVD, and IS metrics. During inference, we apply classifier-free guidance with a scale of 1.2 for the GPDiT-H model and 2.0 for the GPDiT-B model.

**Main results.** Table 2 shows GPDiT achieves a competitive FID of 7.4 and an FVD of 68 on MSR-VTT, demonstrating its effectiveness in handling diverse video generation tasks without direct



Figure 4: Video generation of the subsequent 16 frames conditioned on the initial 13 frames from the MovieGenBenchmark dataset, with the frames sampled at three-frame intervals thereafter. For more details, zoom in to observe finer aspects of the generation process.

Table 2: *Zero-Shot* performance comparison of video generation on MSRVTT and UCF-101, 12-frame video sequences are generated, conditioned on 5 input frames.

Dataset	Method	#Data	#Params	FID ↓	FVD ↓	IS ↑
MSRVTT	MagicVideo [59]	10M	-	36.5	998	-
	LVDM [11]	2M	1.2B	-	742	-
	ModelScope [47]	10M	1.7B	-	550	-
	PixelDance [57]	10M	1.5B	-	381	-
	DreamVideo [46]	5.3M+340k	2.0B	-	149	-
	SnapVideo [30]	1.1B	3.9B	8.5	110	-
	GPDiT-H	192M Img + 6.4M Vid	2.0B	<b>7.4</b>	<b>68</b>	-
	GPDiT-H-LONG	24M Vid	2.0B	<b>7.4</b>	<b>64</b>	-
UCF-101	MagicVideo [59]	10M	-	145.0	699	-
	CogVideo [15]	5.4M	9B	-	626	50.5
	InternVid [50]	28M	-	60.3	617	21.0
	Video-LDM [2]	10M	4.2B	-	551	33.5
	Make-A-Video [38]	20M	9.7B	-	367	33.0
	SnapVideo [30]	1.1B	3.9B	39.0	260	-
	PixelDance [57]	10M	1.5B	49.4	<b>243</b>	42.1
	GPDiT-H	192M Img + 6.4M Vid	2.0B	<b>14.8</b>	<b>243</b>	<b>66.5</b>
	GPDiT-H-LONG	24M Vid	2.0B	<b>7.9</b>	<b>218</b>	<b>66.6</b>

exposure to the test data. Moreover, GPDiT consistently outperforms previous methods in both FID and FVD, underscoring its potential to handle a wide range of unseen video data. On UCF-101, GPDiT also performs well across metrics, with an IS of 66.5, FID of 14.8, and FVD of 243. Notably, GPDiT-H-LONG, trained with 24M video data, achieves the best results with an IS of 66.6, FID of 7.9, and FVD of 218, further showcasing the model’s generalization ability. As shown in Table 3, both GPDiT-B-OF2 and GPDiT-B-OF achieve strong alignment with the UCF-101 distribution, attaining competitive FVD scores of 214 and 216 respectively with only 80M parameters. These results validate GPDiT’s effectiveness in distribution fitting and its consistent robustness across varying model scales. For visual demonstration, we present the generated videos derived from 13 input frames alongside their corresponding 16-frame extensions on the MovieGenBench dataset [32], as shown in Figure 4.

### 5.3 Video representation

To assess the model’s representation ability, we conduct linear probing experiments with two attention mechanisms, extracting features from various layers of GPDiT-B and GPDiT-H. It is important to note that GPDiT-B is trained on UCF-101, while GPDiT-H is trained on close-source open-



domain dataset, so the representation ability measured is both fit and generalized. The probing task is constructed by globally pooling features extracted from the frozen GPDiT model and training a logistic layer for the UCF-101 classification task. For each sample, we uniformly select 13 frames, spaced three frames apart, and pass them through the backbone without temporal rotation.

**Main results.** Figure 5a shows the classification accuracy for two different attention mechanisms on the GPDiT-B model. Notably, OF2 outperforms OF by a significant margin, highlighting the enhanced representation performance when allowing interactions between clean context frames. This aligns with intuition, as interactions between clean frames enhance the model’s ability to understand the content. We also observe that the classification accuracy tends to peak at earlier layers, initially rising at shallow layers before gradually declining. This is consistent with the classification results presented in REPA [56], where enhanced representation ability strengthens fitting in the shallow layers. This further demonstrates GPDiT’s ability to fit and improve representation quality. Figure 5b illustrates the classification accuracy of GPDiT-H-OF2 across different training steps and layers. As training progresses, the classification accuracy steadily improves. Additionally, since GPDiT-H-OF2 is zero-shot on the UCF-101 dataset, accuracy peaks at the 2/3 layer, which is inconsistent with the results of GPDiT-B. Figure 5c demonstrates the correlation between the generation metric (FVD) and classification accuracy for GPDiT-H-OF2. There is a clear positive correlation between generative capability and representational ability, indicating that as training progresses, both the generative performance and the representation ability of GPDiT improve simultaneously.

Table 3: FVD comparison of methods trained on UCF-101.

Model	#Params	Type	FVD
ExtDM-K2 [58]	119 M	Video-DIT	394
OmniTokenizer [49]	227M	Token-AR	314
ACDiT [17]	130M	Frame-AR	376
MAGI [61]	850M	Frame-AR	297
FAR [10]	130M	Frame-AR	194
GPDiT-B-OF	80M	Frame-AR	216
GPDiT-B-OF2	80M	Frame-AR	214

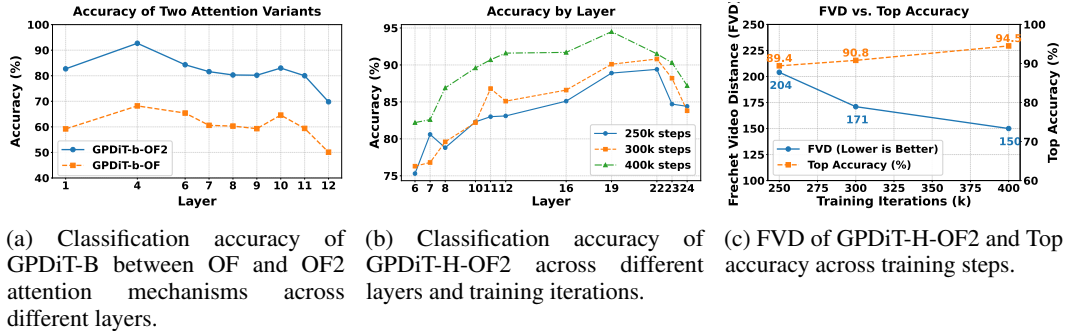


Figure 5: Linear probing performance of GPDiT across different training settings.

## 5.4 Video Few-shot Learning

The pre-trained GPDiT exhibits strong representational ability, and our AR paradigm enables conditioning via sequence concatenation, allowing easy generalization to other tasks without the need for additional modules like VACE [19] or IP-Adapter [54]. This motivates the investigation of the few-shot learning capabilities of pre-trained models across multiple tasks, including grayscale conversion, depth estimation, human detection, image colorization, canny edge-to-image reconstruction, and two style transfer applications. The pretrained GPDiT-H model undergoes 500 iterations of fine-tuning with a batch size of 4, optimized to generate transformations conditioned on both input images and contextual demonstrations. During testing, the model uses two (source, target) pairs as dynamic conditioning inputs to generate the transformed output for an unseen source image.

**Main results.** Figure 6 and Figure 7 show that GPDiT is able to transfer to multiple downstream tasks after few-shot learning. It is clearly demonstrated that GPDiT can easily convert color images to black-and-white and vice versa. In the Human Detection task, the model accurately distinguishes the number of people and their body skeleton. Additionally, it supports controllable editing by generating



controlled instances using edge maps. For instance, Figure 7 shows that the bird generated in the Canny Edge to Image task follows the contours with fine detail. We also explored popular style transfers, such as TikTok-style face-to-cartoon transformations and GPT4o-Ghibli art style switches (Figure 7). Additionally, since only 20 shots are needed for few-shot learning, similar to GPT-2, this suggests the potential for larger GPDiT models to exhibit emergent In-Context Learning (ICL) abilities, as seen in the transition from GPT-2 to GPT-3.

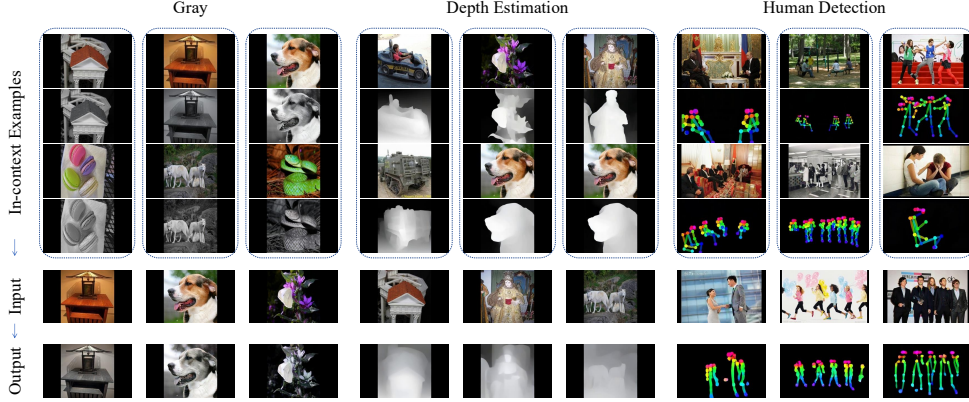


Figure 6: Extracting Low Information from Images: Skeleton, Depth, and Grayscale Transformations.

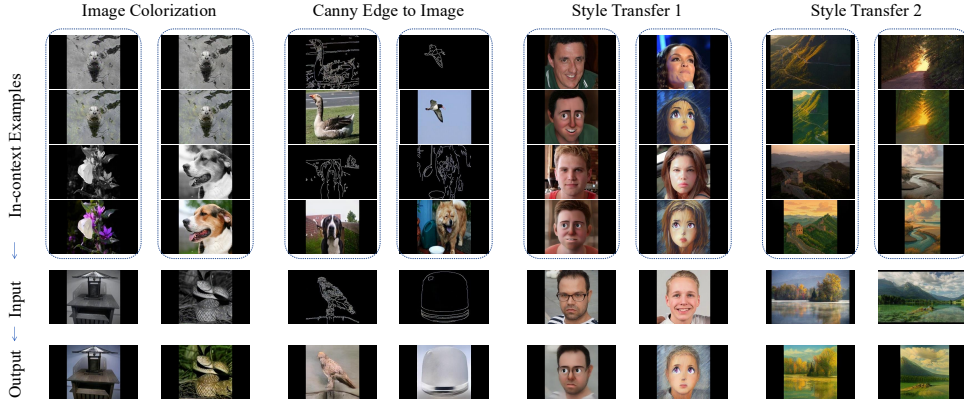


Figure 7: Results of Style Transfer and Conditional Generation: Image Colorization, Edge-to-Image and Two Style Transfer Tasks.

## 6 Discussion

In this work, we present a novel framework that unifies autoregressive modeling and diffusion for video generation. Our method incorporates a lightweight attention mechanism that leverages temporal redundancy to reduce computational overhead, as well as a parameter-free, rotation-based time-conditioning strategy to efficiently inject temporal information. These design choices enable faster training and inference without sacrificing model performance. Extensive experiments demonstrate that our model achieves state-of-the-art performance in video generation, competitive results in video representation, and robust generalization in few-shot multi-task settings, underscoring its versatility across various video modeling tasks.

**Limitations.** Due to resource constraints, we are unable to scale our experiments to larger configurations. In future work, we plan to explore larger-scale models and investigate their potential for in-context learning. While our model demonstrates strong representational capabilities, it is currently limited to the video modality. The design choice of conditioning along the sequence dimension enables seamless integration of other modalities, allowing natural extensibility to multi-modal inputs, such as language. We intend to explore this unified generative-understanding model in future research.

## References

- [1] Andreas Blattmann, Tim Dockhorn, Sumith Kulal, Daniel Mendelevitch, Maciej Kilian, Dominik Lorenz, Yam Levi, Zion English, Vikram Voleti, Adam Letts, et al. Stable video diffusion: Scaling latent video diffusion models to large datasets. *arXiv preprint arXiv:2311.15127*, 2023.
- [2] Andreas Blattmann, Robin Rombach, Huan Ling, Tim Dockhorn, Seung Wook Kim, Sanja Fidler, and Karsten Kreis. Align your latents: High-resolution video synthesis with latent diffusion models. In *Proceedings of the IEEE/CVF conference on computer vision and pattern recognition*, pages 22563–22575, 2023.
- [3] Tom Brown, Benjamin Mann, Nick Ryder, Melanie Subbiah, Jared D Kaplan, Prafulla Dhariwal, Arvind Neelakantan, Pranav Shyam, Girish Sastry, Amanda Askell, et al. Language models are few-shot learners. *Advances in neural information processing systems*, 33:1877–1901, 2020.
- [4] Jake Bruce, Michael D Dennis, Ashley Edwards, Jack Parker-Holder, Yuge Shi, Edward Hughes, Matthew Lai, Aditi Mavalankar, Richie Steigerwald, Chris Apps, et al. Genie: Generative interactive environments. In *Forty-first International Conference on Machine Learning*, 2024.
- [5] Boyuan Chen, Diego Martí Monsó, Yilun Du, Max Simchowitz, Russ Tedrake, and Vincent Sitzmann. Diffusion forcing: Next-token prediction meets full-sequence diffusion. *Advances in Neural Information Processing Systems*, 37:24081–24125, 2024.
- [6] Junsong Chen, Jincheng Yu, Chongjian Ge, Lewei Yao, Enze Xie, Yue Wu, Zhongdao Wang, James Kwok, Ping Luo, Huchuan Lu, et al. Pixart- $\alpha$ : Fast training of diffusion transformer for photorealistic text-to-image synthesis. *arXiv preprint arXiv:2310.00426*, 2023.
- [7] Haoge Deng, Ting Pan, Haiwen Diao, Zhengxiong Luo, Yufeng Cui, Huchuan Lu, Shiguang Shan, Yonggang Qi, and Xinlong Wang. Autoregressive video generation without vector quantization. *arXiv preprint arXiv:2412.14169*, 2024.
- [8] Kaifeng Gao, Jiaxin Shi, Hanwang Zhang, Chunping Wang, and Jun Xiao. Vid-gpt: Introducing gpt-style autoregressive generation in video diffusion models. *arXiv preprint arXiv:2406.10981*, 2024.
- [9] Songwei Ge, Thomas Hayes, Harry Yang, Xi Yin, Guan Pang, David Jacobs, Jia-Bin Huang, and Devi Parikh. Long video generation with time-agnostic vqgan and time-sensitive transformer. In *European Conference on Computer Vision*, pages 102–118. Springer, 2022.
- [10] Yuchao Gu, Weijia Mao, and Mike Zheng Shou. Long-context autoregressive video modeling with next-frame prediction. *arXiv preprint arXiv:2503.19325*, 2025.
- [11] Yingqing He, Tianyu Yang, Yong Zhang, Ying Shan, and Qifeng Chen. Latent video diffusion models for high-fidelity long video generation. *arXiv preprint arXiv:2211.13221*, 2022.
- [12] Martin Heusel, Hubert Ramsauer, Thomas Unterthiner, Bernhard Nessler, and Sepp Hochreiter. Gans trained by a two time-scale update rule converge to a local nash equilibrium. *Advances in neural information processing systems*, 30, 2017.
- [13] Jonathan Ho, Ajay Jain, and Pieter Abbeel. Denoising diffusion probabilistic models. *Advances in neural information processing systems*, 33:6840–6851, 2020.
- [14] Jonathan Ho, Tim Salimans, Alexey Gritsenko, William Chan, Mohammad Norouzi, and David J Fleet. Video diffusion models. *Advances in Neural Information Processing Systems*, 35:8633–8646, 2022.
- [15] Wenyi Hong, Ming Ding, Wendi Zheng, Xinghan Liu, and Jie Tang. Cogvideo: Large-scale pretraining for text-to-video generation via transformers. *arXiv preprint arXiv:2205.15868*, 2022.
- [16] Jinyi Hu, Shengding Hu, Yuxuan Song, Yufei Huang, Mingxuan Wang, Hao Zhou, Zhiyuan Liu, Wei-Ying Ma, and Maosong Sun. Acddit: Interpolating autoregressive conditional modeling and diffusion transformer. *arXiv preprint arXiv:2412.07720*, 2024.

- [17] Jinyi Hu, Shengding Hu, Yuxuan Song, Yufei Huang, Mingxuan Wang, Hao Zhou, Zhiyuan Liu, Wei-Ying Ma, and Maosong Sun. Acddit: Interpolating autoregressive conditional modeling and diffusion transformer, 2025.
- [18] Haoyang Huang, Guoqing Ma, Nan Duan, Xing Chen, Changyi Wan, Ranchen Ming, Tianyu Wang, Bo Wang, Zhiying Lu, Aojie Li, et al. Step-video-ti2v technical report: A state-of-the-art text-driven image-to-video generation model. *arXiv preprint arXiv:2503.11251*, 2025.
- [19] Zeyinzi Jiang, Zhen Han, Chaojie Mao, Jingfeng Zhang, Yulin Pan, and Yu Liu. Vace: All-in-one video creation and editing. *arXiv preprint arXiv:2503.07598*, 2025.
- [20] Jihwan Kim, Junoh Kang, Jinyoung Choi, and Bohyung Han. Fifo-diffusion: Generating infinite videos from text without training. *arXiv preprint arXiv:2405.11473*, 2024.
- [21] Dan Kondratyuk, Lijun Yu, Xiuye Gu, José Lezama, Jonathan Huang, Grant Schindler, Rachel Hornung, Vighnesh Birodkar, Jimmy Yan, Ming-Chang Chiu, et al. Videopoet: A large language model for zero-shot video generation. *arXiv preprint arXiv:2312.14125*, 2023.
- [22] Weijie Kong, Qi Tian, Zijian Zhang, Rox Min, Zuozhuo Dai, Jin Zhou, Jiangfeng Xiong, Xin Li, Bo Wu, Jianwei Zhang, et al. Hunyuanvideo: A systematic framework for large video generative models. *arXiv preprint arXiv:2412.03603*, 2024.
- [23] Yaron Lipman, Ricky TQ Chen, Heli Ben-Hamu, Maximilian Nickel, and Matt Le. Flow matching for generative modeling. *arXiv preprint arXiv:2210.02747*, 2022.
- [24] Xingchao Liu, Chengyue Gong, and Qiang Liu. Flow straight and fast: Learning to generate and transfer data with rectified flow. *arXiv preprint arXiv:2209.03003*, 2022.
- [25] Yaofang Liu, Yumeng Ren, Xiaodong Cun, Aitor Artola, Yang Liu, Tiejong Zeng, Raymond H Chan, and Jean-michel Morel. Redefining temporal modeling in video diffusion: The vectorized timestep approach. *arXiv preprint arXiv:2410.03160*, 2024.
- [26] Zhengxiong Luo, Dayou Chen, Yingya Zhang, Yan Huang, Liang Wang, Yujun Shen, Deli Zhao, Jingren Zhou, and Tieniu Tan. Videofusion: Decomposed diffusion models for high-quality video generation. *arXiv preprint arXiv:2303.08320*, 2023.
- [27] Guoqing Ma, Haoyang Huang, Kun Yan, Liangyu Chen, Nan Duan, Shengming Yin, Changyi Wan, Ranchen Ming, Xiaoni Song, Xing Chen, et al. Step-video-t2v technical report: The practice, challenges, and future of video foundation model. *arXiv preprint arXiv:2502.10248*, 2025.
- [28] Nanye Ma, Mark Goldstein, Michael S Albergo, Nicholas M Boffi, Eric Vanden-Eijnden, and Saining Xie. Sit: Exploring flow and diffusion-based generative models with scalable interpolant transformers. In *European Conference on Computer Vision*, pages 23–40. Springer, 2024.
- [29] Xin Ma, Yaohui Wang, Gengyun Jia, Xinyuan Chen, Ziwei Liu, Yuan-Fang Li, Cunjian Chen, and Yu Qiao. Latte: Latent diffusion transformer for video generation. *arXiv preprint arXiv:2401.03048*, 2024.
- [30] Willi Menapace, Aliaksandr Siarohin, Ivan Skorokhodov, Ekaterina Deyneka, Tsai-Shien Chen, Anil Kag, Yuwei Fang, Aleksei Stoliar, Elisa Ricci, Jian Ren, and Sergey Tulyakov. Snap video: Scaled spatiotemporal transformers for text-to-video synthesis, 2024.
- [31] William Peebles and Saining Xie. Scalable diffusion models with transformers. In *Proceedings of the IEEE/CVF international conference on computer vision*, pages 4195–4205, 2023.
- [32] Adam Polyak, Amit Zohar, Andrew Brown, Andros Tjandra, Animesh Sinha, Ann Lee, Apoorv Vyas, Bowen Shi, Chih-Yao Ma, Ching-Yao Chuang, David Yan, Dhruv Choudhary, DingKang Wang, Geet Sethi, Guan Pang, Haoyu Ma, Ishan Misra, Ji Hou, Jialiang Wang, Kiran Jagadeesh, Kunpeng Li, Luxin Zhang, Mannat Singh, Mary Williamson, Matt Le, Matthew Yu, Mitesh Kumar Singh, Peizhao Zhang, Peter Vajda, Quentin Duval, Rohit Girdhar, Roshan Sumbaly, Sai Saketh Rambhatla, Sam Tsai, Samaneh Azadi, Samyak Datta, Sanyuan Chen, Sean Bell, Sharadh Ramaswamy, Shelly Sheynin, Siddharth Bhattacharya, Simran Motwani,

- Tao Xu, Tianhe Li, Tingbo Hou, Wei-Ning Hsu, Xi Yin, Xiaoliang Dai, Yaniv Taigman, Yaqiao Luo, Yen-Cheng Liu, Yi-Chiao Wu, Yue Zhao, Yuval Kirstain, Zecheng He, Zijian He, Albert Pumarola, Ali Thabet, Artsiom Sanakoyeu, Arun Mallya, Baishan Guo, Boris Araya, Breana Kerr, Carleigh Wood, Ce Liu, Cen Peng, Dmitry Vengertsev, Edgar Schonfeld, Elliot Blanchard, Felix Juefei-Xu, Fraylie Nord, Jeff Liang, John Hoffman, Jonas Kohler, Kaolin Fire, Karthik Sivakumar, Lawrence Chen, Licheng Yu, Luya Gao, Markos Georgopoulos, Rashel Moritz, Sara K. Sampson, Shikai Li, Simone Parmeggiani, Steve Fine, Tara Fowler, Vladan Petrovic, and Yuming Du. Movie gen: A cast of media foundation models, 2025.
- [33] Reiner Pope, Sholto Douglas, Aakanksha Chowdhery, Jacob Devlin, James Bradbury, Jonathan Heek, Kefan Xiao, Shivani Agrawal, and Jeff Dean. Efficiently scaling transformer inference. *Proceedings of Machine Learning and Systems*, 5:606–624, 2023.
  - [34] Alec Radford, Karthik Narasimhan, Tim Salimans, Ilya Sutskever, et al. Improving language understanding by generative pre-training. 2018.
  - [35] Alec Radford, Jeffrey Wu, Rewon Child, David Luan, Dario Amodei, Ilya Sutskever, et al. Language models are unsupervised multitask learners. *OpenAI blog*, 1(8):9, 2019.
  - [36] Tim Salimans, Ian Goodfellow, Wojciech Zaremba, Vicki Cheung, Alec Radford, and Xi Chen. Improved techniques for training gans. *Advances in neural information processing systems*, 29, 2016.
  - [37] Christoph Schuhmann, Romain Beaumont, Richard Vencu, Cade Gordon, Ross Wightman, Mehdi Cherti, Theo Coombes, Aarush Katta, Clayton Mullis, Mitchell Wortsman, et al. Laion-5b: An open large-scale dataset for training next generation image-text models. *Advances in neural information processing systems*, 35:25278–25294, 2022.
  - [38] Uriel Singer, Adam Polyak, Thomas Hayes, Xi Yin, Jie An, Songyang Zhang, Qiyuan Hu, Harry Yang, Oron Ashual, Oran Gafni, et al. Make-a-video: Text-to-video generation without text-video data. *arXiv preprint arXiv:2209.14792*, 2022.
  - [39] Kiwhan Song, Boyuan Chen, Max Simchowitz, Yilun Du, Russ Tedrake, and Vincent Sitzmann. History-guided video diffusion. *arXiv preprint arXiv:2502.06764*, 2025.
  - [40] Yang Song, Jascha Sohl-Dickstein, Diederik P Kingma, Abhishek Kumar, Stefano Ermon, and Ben Poole. Score-based generative modeling through stochastic differential equations. *arXiv preprint arXiv:2011.13456*, 2020.
  - [41] Khurram Soomro, Amir Roshan Zamir, and Mubarak Shah. Ucf101: A dataset of 101 human actions classes from videos in the wild. *arXiv preprint arXiv:1212.0402*, 2012.
  - [42] Mingzhen Sun, Weining Wang, Gen Li, Jiawei Liu, Jiahui Sun, Wanquan Feng, Shanshan Lao, SiYu Zhou, Qian He, and Jing Liu. Ar-diffusion: Asynchronous video generation with auto-regressive diffusion. *arXiv preprint arXiv:2503.07418*, 2025.
  - [43] Mingzhen Sun, Weining Wang, Xinxin Zhu, and Jing Liu. Moso: Decomposing motion, scene and object for video prediction. In *Proceedings of the IEEE/CVF conference on computer vision and pattern recognition*, pages 18727–18737, 2023.
  - [44] Thomas Unterthiner, Sjoerd Van Steenkiste, Karol Kurach, Raphaël Marinier, Marcin Michalski, and Sylvain Gelly. Fvd: A new metric for video generation. 2019.
  - [45] Ang Wang, Baole Ai, Bin Wen, Chaojie Mao, Chen-Wei Xie, Di Chen, Feiwei Yu, Haiming Zhao, Jianxiao Yang, Jianyuan Zeng, et al. Wan: Open and advanced large-scale video generative models. *arXiv preprint arXiv:2503.20314*, 2025.
  - [46] Cong Wang, Jiayi Gu, Panwen Hu, Yuanfan Guo, Xiao Dong, Hang Xu, and Xiaodan Liang. Dreamvideo: High-fidelity image-to-video generation with image retention and text guidance. In *ICASSP 2025-2025 IEEE International Conference on Acoustics, Speech and Signal Processing (ICASSP)*, pages 1–5. IEEE, 2025.
  - [47] Jiuniu Wang, Hangjie Yuan, Dayou Chen, Yingya Zhang, Xiang Wang, and Shiwei Zhang. Modelscope text-to-video technical report. *arXiv preprint arXiv:2308.06571*, 2023.

- [48] Junke Wang, Yi Jiang, Zehuan Yuan, Bingyue Peng, Zuxuan Wu, and Yu-Gang Jiang. Omnitokenizer: A joint image-video tokenizer for visual generation. *Advances in Neural Information Processing Systems*, 37:28281–28295, 2024.
- [49] Junke Wang, Yi Jiang, Zehuan Yuan, Binyue Peng, Zuxuan Wu, and Yu-Gang Jiang. Omnitokenizer: A joint image-video tokenizer for visual generation, 2024.
- [50] Yi Wang, Yanan He, Yizhuo Li, Kunchang Li, Jiashuo Yu, Xin Ma, Xinhao Li, Guo Chen, Xinyuan Chen, Yaohui Wang, et al. Internvid: A large-scale video-text dataset for multimodal understanding and generation. *arXiv preprint arXiv:2307.06942*, 2023.
- [51] Desai Xie, Zhan Xu, Yicong Hong, Hao Tan, Difan Liu, Feng Liu, Arie Kaufman, and Yang Zhou. Progressive autoregressive video diffusion models. *arXiv preprint arXiv:2410.08151*, 2024.
- [52] Jun Xu, Tao Mei, Ting Yao, and Yong Rui. Msr-vtt: A large video description dataset for bridging video and language. In *Proceedings of the IEEE conference on computer vision and pattern recognition*, pages 5288–5296, 2016.
- [53] Wilson Yan, Yunzhi Zhang, Pieter Abbeel, and Aravind Srinivas. Videogpt: Video generation using vq-vae and transformers. *arXiv preprint arXiv:2104.10157*, 2021.
- [54] Hu Ye, Jun Zhang, Sibio Liu, Xiao Han, and Wei Yang. Ip-adapter: Text compatible image prompt adapter for text-to-image diffusion models. *arXiv preprint arXiv:2308.06721*, 2023.
- [55] Lijun Yu, José Lezama, Nitesh B Gundavarapu, Luca Versari, Kihyuk Sohn, David Minnen, Yong Cheng, Vighnesh Birodkar, Agrim Gupta, Xiuye Gu, et al. Language model beats diffusion-tokenizer is key to visual generation. *arXiv preprint arXiv:2310.05737*, 2023.
- [56] Sihyun Yu, Sangkyung Kwak, Huiwon Jang, Jongheon Jeong, Jonathan Huang, Jinwoo Shin, and Saining Xie. Representation alignment for generation: Training diffusion transformers is easier than you think. *arXiv preprint arXiv:2410.06940*, 2024.
- [57] Yan Zeng, Guoqiang Wei, Jiani Zheng, Jiaxin Zou, Yang Wei, Yuchen Zhang, and Hang Li. Make pixels dance: High-dynamic video generation, 2023.
- [58] Zhicheng Zhang, Junyao Hu, Wentao Cheng, Danda Paudel, and Jufeng Yang. Extdm: Distribution extrapolation diffusion model for video prediction. In *Proceedings of the IEEE/CVF Conference on Computer Vision and Pattern Recognition*, pages 19310–19320, 2024.
- [59] Daquan Zhou, Weimin Wang, Hanshu Yan, Weiwei Lv, Yizhe Zhu, and Jiashi Feng. Magicvideo: Efficient video generation with latent diffusion models. *arXiv preprint arXiv:2211.11018*, 2022.
- [60] Deyu Zhou, Quan Sun, Yuang Peng, Kun Yan, Runpei Dong, Duomin Wang, Zheng Ge, Nan Duan, Xiangyu Zhang, Lionel M Ni, et al. Taming teacher forcing for masked autoregressive video generation. *arXiv preprint arXiv:2501.12389*, 2025.
- [61] Deyu Zhou, Quan Sun, Yuang Peng, Kun Yan, Runpei Dong, Duomin Wang, Zheng Ge, Nan Duan, Xiangyu Zhang, Lionel M. Ni, and Heung-Yeung Shum. Taming teacher forcing for masked autoregressive video generation, 2025.

## A Additional Experimental Details and Results

### A.1 Video generation results

We begin by evaluating the effect of our lightweight attention variant on training convergence, in comparison to standard causal attention. As shown in Figure 8, the OF2 model exhibits a slight improvement in training convergence speed compared to the OF one.

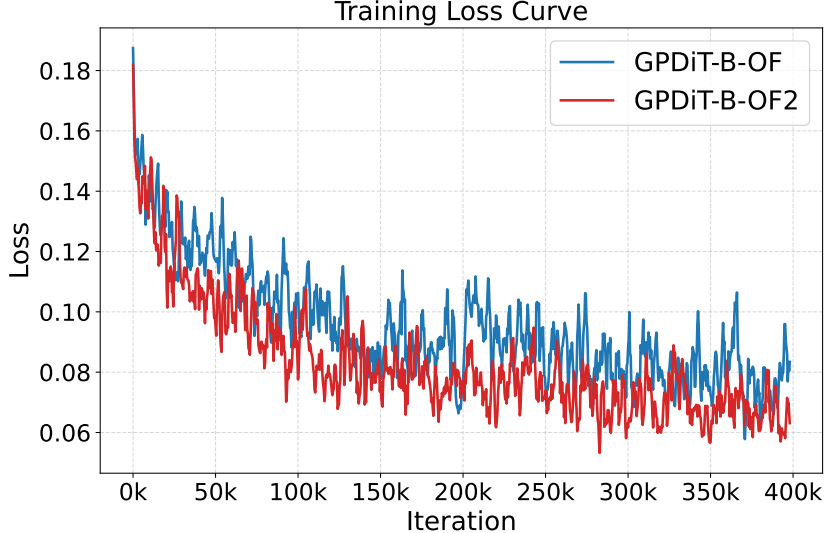


Figure 8: Training loss comparison of GPDiT-B-OF2 and GPDiT-B-OF.

Figure 9 and Figure 10 showcase video prediction results conditioned on camera motion. Each example is generated from 13 input frames and extended by 16 predicted frames, sampled at every fourth frame from the MovieGenBench dataset. The top row presents the ground truth, and the bottom row shows the predicted frames. These examples demonstrate the model’s ability to accurately anticipate dynamic camera movements and physical scene transitions.

### A.2 Visual Question Answering results

To further validate the discriminative capability of our model’s representations, we replace the vision encoder pretrained CLIP in Video-ChatGPT [?] with the first 18 layers of our trained GPDiT-H model as the feature extractor. Correspondingly, we replace the original linear layer with a new linear layer matching the output dimensions of GPDiT-H. Following the standard practice of Video-ChatGPT, we freeze the parameters of the feature extractor and train only the linear layer. The training batch size is set to 4, the learning rate is set to  $2e-5$ , and the number of training epochs is 6.

It is worth noting that our model is not trained in language modality and solely based on video modality for representation learning. Despite this, as illustrated in Table 4, our model achieves an accuracy of 28.2% on ActivityNet-QA, compared to the original 35.2%. This result further validates the competitive discriminative capability of our model’s representations, demonstrating promising potential for future multi-modality integration and training.

Table 4: Activity Net-QA

Model	Accuracy	Score
Video-ChatGPT	35.2	2.8
GPDiT-H-OF2-Long	28.2	1.54



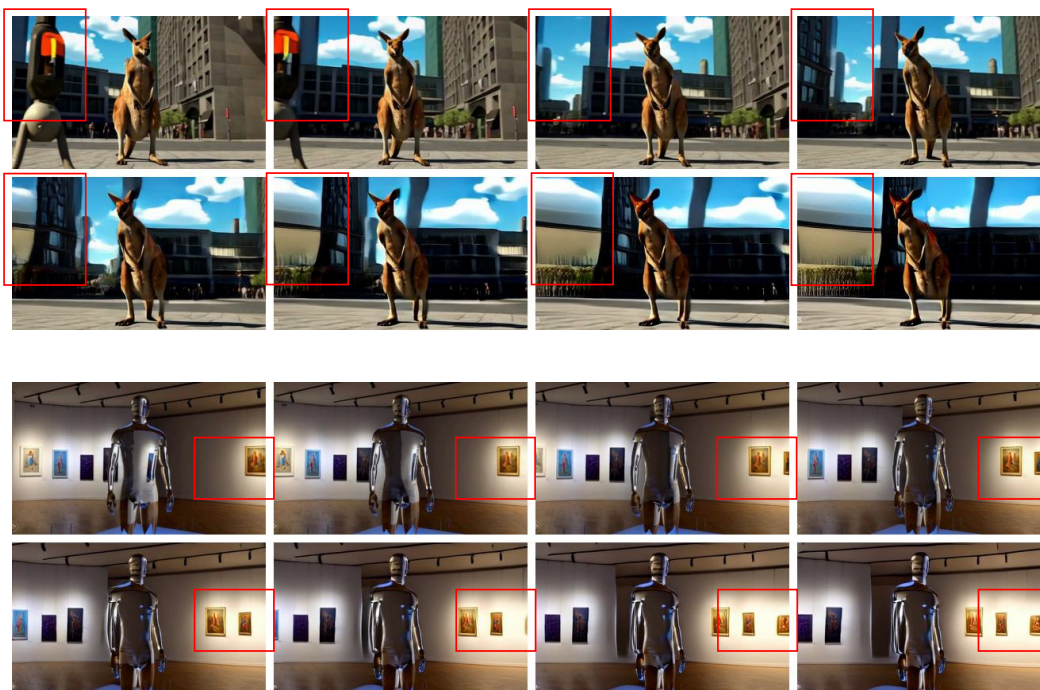


Figure 9: Camera Motion Control Prediction (Camera Rotation).



Figure 10: Camera Motion Control Prediction (First: Far-to-Near, Second: Left-to-Right).